Induction of Highly Ordered Liquid Crystalline Phase of an Azobenzene side chain polymer by Contact with 4'-pentyl-4-cyanobiphenyl; An in Situ Study

Chikara Kawakami[1], Mitsuo Hara[1], Shusaku Nagano[2], and Takahiro Seki*[1]*

[1] Department of Molecular and Macromolecular Chemistry, Graduate School of Engineering, Nagoya University, Furo-cho, Chikusa-ku, Nagoya, Aichi 464-8603, Japan

[2]Department of Chemistry, College of Science, Rikkyo University, 3-34-1 Nishi-Ikebukuro, Toshima, Tokyo 171-8501, Japan

Corresponding Authors:
mhara@chembio.nagoya-u.ac.jp (M. H.) and tseki@chembio.nagoya-u.ac.jp (T. S.)

KEYWORDS: thermotropic liquid crystal, smectic phase, azobenzene, command surface, solid interface

for Table of Contents use only

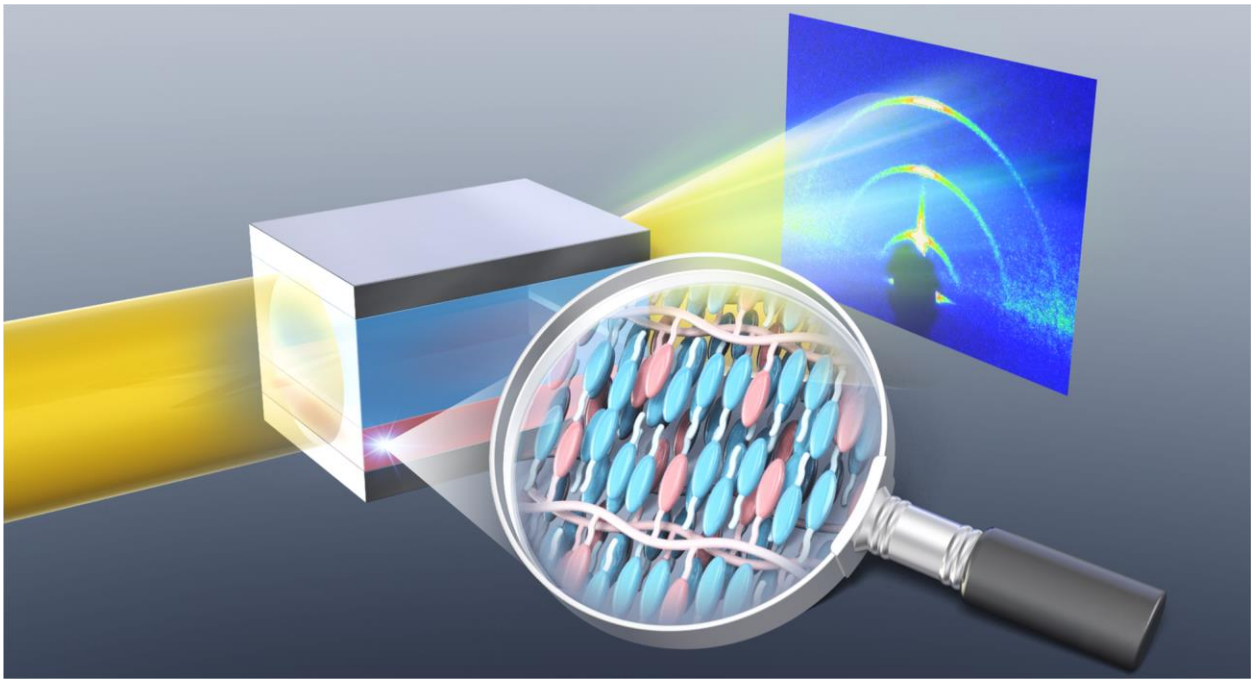

ABSTRACT:

The orientation of liquid crystal (LC) molecules is significantly governed by solid interfaces and free surfaces, and a variety of functional materials have been developed using these properties. Although LC materials are already in industrial use, particularly for LC display panels, various studies have been conducted in recent years to better grasp the interface behavior of LC molecules. In this work, we succeeded in in situ observations of induction of higher ordered LC phases at the interface between a side-chain LC azobenzene polymer film with a thickness of ~400 nm and a low-molecular-mass nematic LC, 4'-pentyl-4-cyanobiphenyl of 35 μm thickness, using small-angle X-ray scattering measurements and polarized optical microscopy. It is revealed that the two different mesogens cooperatively form hybrid higher ordered smectic LC phases probably through weak electron transfer immediately after interfacial contact. The induction process consists of three stages in terms of dynamic structure evolutions. Upon UV irradiation, the hybrid smectic LC structure diminished. This study provides new insights into the behavior of LC molecules near the alignment film on the solid substrate.

INTRODUCTION

The cooperativity of liquid crystals (LCs) plays an important role in controlling molecular orientation on a macroscopic scale. LCs are utilized for creation of many functional materials, such as light-driven actuators, and optical devices.[1-8] Generally, the orientation of LC molecules are highly sensitive to the surface free energy, surface roughness, and dielectric constant and molecular structure of the interface, and thus, many interface-mediated processes have been proposed to align LC molecules and their assembled structures.[9–25] LC displays (LCDs), which have grown as a major industrial production since their invention, require sophisticated surface control technology. Thus, over the past 50 years, numerous LC alignment technologies have been proposed and developed to precisely control the orientation of nematic LCs (NLCs).[26–30]

Optical alignment switching of low-molecular-mass NLC orientation was first demonstrated in 1988 using an azobenzene (Az) molecular layers attached onto a solid substrate.[31] Such light-driven NLC alignment systems are often called as “command surfaces”,[32-34] Recent studies have demonstrated that the photoresponsive layer at the free surface can work as the command layer for side chain liquid crystalline polymer (SCLCP) films.[35-38] In spite of accumulated data on the surface control of LC materials, precise understandings on the anchoring behavior and structuring are still needed. The anchoring behavior of LC molecules in the vicinity of polymer surfaces[39,40] and light-controllable command surfaces remain topics of academic interest, as exemplified by recent demonstrations of the unique orientation behavior of LC molecules near the Az polymer interface.[41-46] Approaches of the computer simulation further deepen understandings of low-molecular-mass LC molecules at interfaces.[47,48]

When an Az side chain polymer is employed as the command layer,[32,33] the elucidation of cooperativity behavior between the polymer layer and NLC is of keen interest. However, in a LC cell system, the majority number NLC molecules in the cell hampers the selective observation of interface regions. In this context, Ubukata et al. explored a model system using Langmuir-Blodgett films of hybrids consisting of an amphiphilic Az side chain polymer and 4-cyano-4'-pentylbiphenyl (5CB).[49,50] Strong molecular cooperativity has been observed in the orientation

changes as confirmed by UV-visible absorption and infrared spectroscopy. Still, detailed experimental information particularly in a time-course dynamic aspect has not been obtained.

We have recently developed a small-angle X-ray scattering (SAXS) measurement technique to evaluate the structure inside a LC-injected sandwich cell.In this technique, an X-ray beam is passed through the LC cell in the cell plane direction.[51,52] This approach allows an in situ observation of structural changes of LC orientation. In this work, we applied this technique to the interface between a side-chain liquid crystalline Az polymer (PAz) and 5CB. As a result, we have elucidated that highly ordered smectic LC phases are induced via hybridization of the PAz and 5CB mesogens. The smectic layer formation allows for the selective and time-course detection of structuring and orientation of mesogens at the interface because the NLC phase that occupies the major volume of LC cell is essentially indetectable by the X-ray measurement. This paper reports, for the first time, the details on the time-course events of NLC contact-induced structuring of the surface LC Az polymer layer. UV light irradiation to this cell has further been conducted to grasp the light induced changes.

EXPERIMENTAL SECTION

The structures of the chemicals used in this study are shown in Figure 1a. Low-molecular-mass nematic liquid crystal, 5CB, was purchased from Tokyo Chemical Industry Co. Ltd.. PAz was synthesized according to a previously reported method[35] (see the Supporting Information).

Figure 1a also displays the LC cell for SAXS measurements and microscope observations. The LC cell was constructed as follows: First, TEMPAX Float® glass substrates with aspect ratios of 1.5 mm × 15.0 mm and 15.0 mm × 15.0 mm and a thickness of 1 mm were purchased. PAz spin-coated films (thickness: ~400 nm) were prepared onto the 15.0 mm × 15.0 mm glass; details of the film preparation are described in the Supporting Information. The resulting films were used as the bottom-side substate of the LC cell. A 35-μm thick Kapton® (polyimide) tape was sandwiched between the 1.5 mm × 15.0 mm glass and used as the cell spacer. The sides of the two substrates were then fixed with UV-curable resin NOA65 (Norland Products Inc.), and the

resulting LC cell was heated at 130 °C for 5 min using a hot plate and then slowly cooled on the hot plate after turning off the heater.

SAXS measurements characterized the self-assembled structure in the LC cell. These measurements were collected using an ultra-bright X-ray generator FR-E (Rigaku Corp.) equipped with a two-dimensional detector (R-AXIS IV, Rigaku). An X-ray beam from Cu Kα radiation (λ = 0.154 nm) was used, and the camera length was set at 292.5 mm. The LC cells were placed onto a pulse motor stage composed of both an oblique pulse (ATS-C310-EM, Chuo Precision Industrial Co. Ltd.) and a Z-pulse (ALV-3005-HM, Chuo Precision Industrial Co. Ltd.) motor. A scintillation counter was set downstream of the LC cells, and the alignment of the LC cells with respect to the incident X-ray beam was adjusted by monitoring with the counter to maximize the X-ray intensity through the cells. The temperature of the LC cells was controlled using a ceramic heater embedded in the stage. Prior to injection of 5CB into the LC cell, both the cell and 5CB were pre-heated at 50 °C using a hot stage. One μL of the hot 5CB was then immediately injected into the cell using a microsyringe. The LC cells were exposed to the X-ray beam for 10 min for each measurement.

Birefringence of the LC cell was observed using a polarized BX51 microscope equipped with a digital camera (DP26, Olympus Corp.). The LC cell was heated at 50 °C using a hot stage (Linkam 10083, Japan High Tech Co. Ltd). Similar to the SAXS measurements, 5CB (1 μL) heated at 50 °C was injected into the LC cell using a microsyringe. After closing the cover of the hot stage, birefringence was observed under crossed Nicols.

UV light irradiation at 365 nm was performed with a LED light source using a CL-1501 (Asahi Spectra Co. Ltd.) at 10 mW cm^{-2} for 120 s. The distance between the light source and the sample was 10 cm.

RESULTS AND DISCUSSION

Figure 1b shows the SAXS images of an empty PAz-coated LC cell before 5CB injection. Two scattering peaks in the out-of-plane direction of the substrate were observed, with *d* values of 2.8 and 1.4 nm. This homeotropic orientation of mesogens can be attained from the free top surface.[35] The *d* values and their ratio indicate that PAz forms the smectic C (SmC) phase.[53] After approximately 2 h from 5CB injection at 50 °C, new scattering peaks of different spacing (*d* = 5.7 and 1.9 nm) were observed in the out-of-plane direction to the substrate (Figure 1c). Thus, the *d* values of all peaks after 5CB injection were 5.7, 2.9, 1.9, and 1.4 nm. We have previously shown that random copolymers containing Az and CB mesogens form a newly and highly ordered hybrid smectic LC phase in the bulk state (reference 54, Figure S5), and similar *d* values have been obtained in this study. These results show that the identical hybrid LC phase was induced by contact with 5CB in the cell. Notably, as mentioned in Figure S1, no scattering was observed when other NLCs, 4'-methyl-4-pentylbiphenyl (5MB) and *N*-(4-methoxybenzylidene)-4-butylaniline (MBBA) were injected instead of 5CB. The hybrid LC phase was observed only when 5CB or 4-cyano-4'-octylbiphenyl (8CB), was used. For the case of low-molecular-mass LC systems, Sugisawa and Tabe[55] reported the formation of a highly ordered hybrid smectic LC phase in in mixtures of Az and cyanobiphenyl (CB) derivatives through a weak charge-transfer interaction between the two mesogens. We suppose that the hybrid LC phase observed at the interface in this study is attributed to the same interaction between the PAz and CB mesogens.

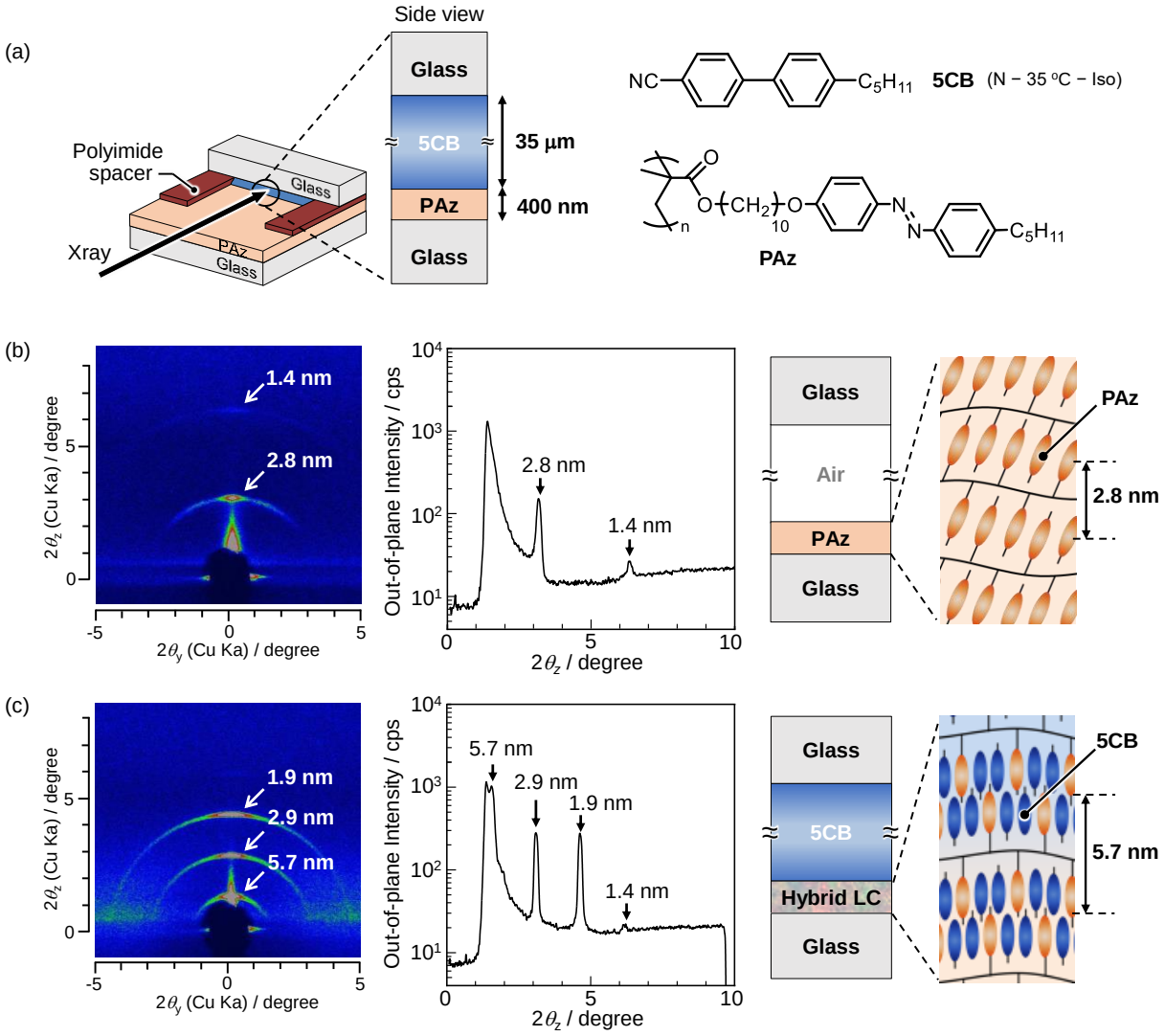

Figure 1. (a) Illustration of the LC cell and chemical structures of the LC materials used in this study. (b, c) 2D SAXS images, out-of-plane intensity profiles, and structural models at 50 °C before (b) and after (c) injection of 5CB into the LC cells.

Time-course changes of the formation process of the hybrid LC phase was first evaluated by polarized optical microscopy (POM) observations and SAXS measurements. Before 5CB injection to the PAz film, slight birefringence was observed (Figure 2a), which should be attributed to the molecular tilt of the PAz mesogens (smectic C phase) to the substrate plane. Immediately after injection of 5CB into the LC cell at 50 °C, the overall birefringence drastically increased and the image became brightened (Figure 2b, also see Movie S1 in the Supporting Information). This indicates that the homeotropic alignment of the PAz mesogens is disturbed and randomized at the moment when the PAz film gets contact with 5CB. Here, this time is defined as 0 min after 5CB injection. After this point, the birefringent character was gradually weakened and the images became darker. In addition, 30 min after 5CB injection, a focal conic pattern was generated (Figure 2c). Notably, in 60 min after 5CB injection, only the focal conic pattern was observed (Figure 2d), which then gradually disappeared (Figure 2e). No birefringent feature was observed after 120 min (Figure 2f). Figure 2g shows the two-dimensional (2D) SAXS image obtained in 4 min after 5 CB injection. Thus, scatterings of the hybrid LC phase were already observed 4 min after 5CB injection. As mentioned, the POM movie (supporting information) also showed a change in the birefringence immediately after 5CB injection. These results suggest that the hybrid LC phase was generated immediately after PAz and 5CB came into contact at 50 °C within the experimental procedure. It is to be noted that the bulk 5CB woth 35 μm thickness in the cell is in the isotropic state (at 50 °C), and thus the observed birefringent character stems from the ordered interface region of PAz and 5CB with 400 nm thickness.

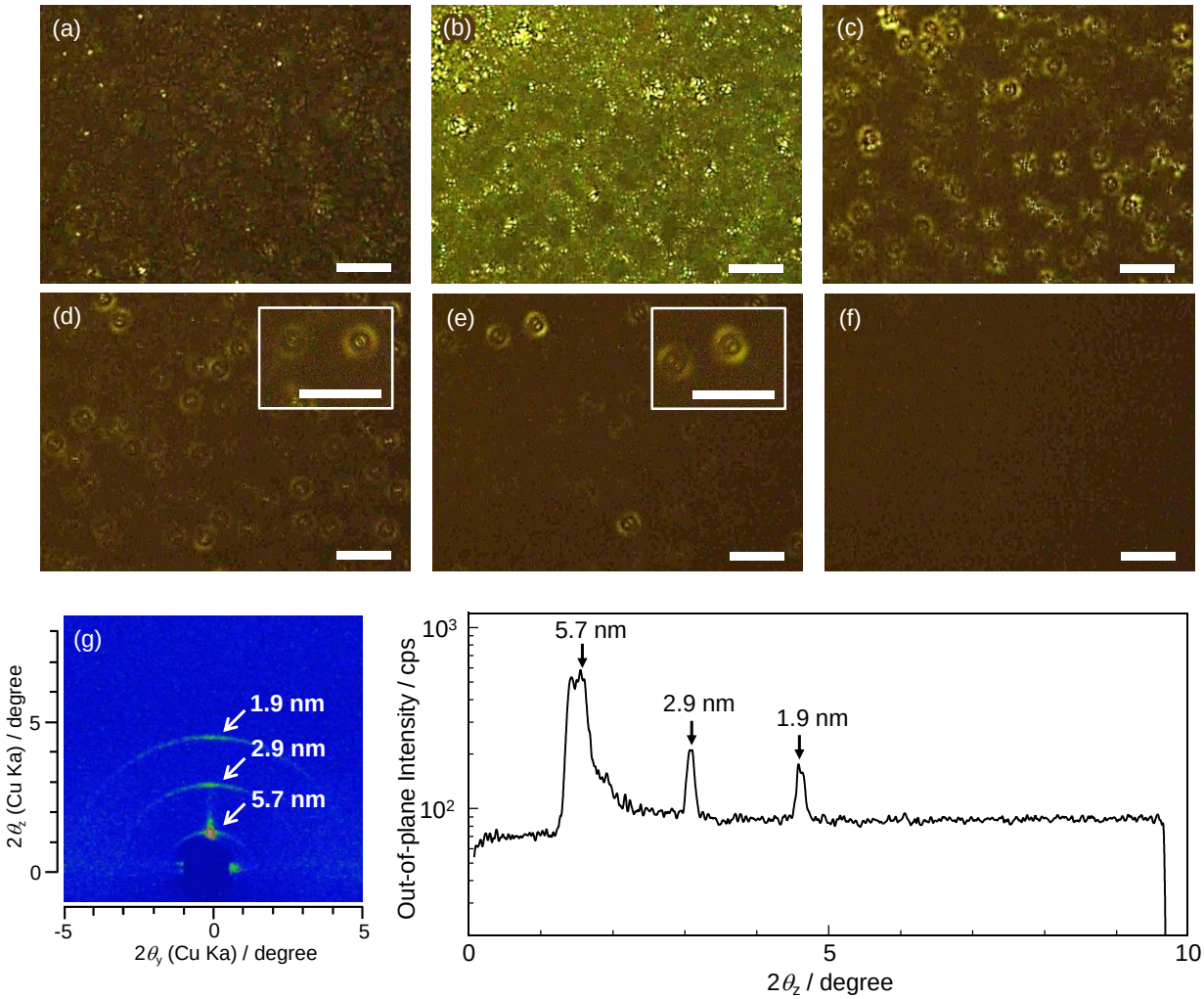

Figure 2. POM images of the LC cell at 50 °C before (a) and after injection of 5CB (b-f) observed with crossed polarizers. (b) immediately (within seconds), (c) 30 min, (d) 60 min, (e) 90 min, and (f) 120 min after injection. Insets in d and e are magnified POM images. Scale bars represent 20 μm. (g) 2D SAXS image of the LC cell at 50 °C 4 min after 5CB injection and its out-of-plane intensity profile (right). Duration of the X-ray beam exposure time was set to 1 min.

Next, time-course changes after injection of 5CB were monitored by SAXS measurements. Figure 3 and Figure S2 show the 2D SAXS images and out-of-plane intensity profiles obtained by SAXS measurements of the LC cells at 14, 70, and 128 min after 5CB injection. As shown in Figure 3a, the *d* value was unchanged with time, however, the scattering intensity increased over time. In fact, focusing on the azimuth angle (ϕ) intensity profiles of the third-order scattering peak (d = 1.9 nm), the maximum intensity increased and the peak became sharper over time (Figure 3b). For this evaluation, the third-order peak was chosen because the comet peak from the substrate affected the baseline up to the second peak.

Plots of the time-course change of the scattering intensity and full width at half maxima (FWHMs, see Figure S3) of the scattering peaks are displayed in Figure 3c. The peak intensities did not change from 0 to 60 min after 5CB injection. Between 60 and 110 min, the intensity increased significantly until they converged to almost the same value after 110 min. On the other hand, the FWHM slightly decreased immediately after injection and showed a rapid reduction around 60 min, and converged to almost the same value after approximately 60 min.

Together with the time-course peak changes of X-ray scattering and POM observations, the structure and orientation behavior of the interfacial hybrid LC phase can be divided into three stages. Figure 3d schematically depicts the hybrid smectic LC phase models at each stage. The hybrid LC phase is immediately formed after the contact, and the structure is characterized as multidomains whose lamellar planes are oriented diversely among these domains (0 – 60 min, Stage I). By keeping at 50 °C, the lamellar planes continuously change their orientation parallel to the substrate with concomitant fusion of the domains (60 – 110 min, Stage II). This orientation of the mesogens changes to a more vertically state, which seems to stem from the memorized initial homeotropic alignment of the PAz mesogens before 5CB injection. The rapid and discontinuous reduction of FWHM should be ascribed to the ordering of the lamellar structure accompanied by the arranged uniform orientation. Subsequently, after 110 min, the defects in the domain decrease significantly as shown by POM observation (Stage III).

It is to be noted that the scattering angle of the second-order peak of the hybrid LC phase ($2\theta_z = 3.1°$) was almost overlapped with that of the first-order peak of the LC phase of pure PAz. Considering a fact that the enhancement ratios of the second- and third-order peaks of the hybrid

LC phase with time were identical, we suppose that the entire parts of PAz film was converted to the hybrid LC phase on contact with 5CB.

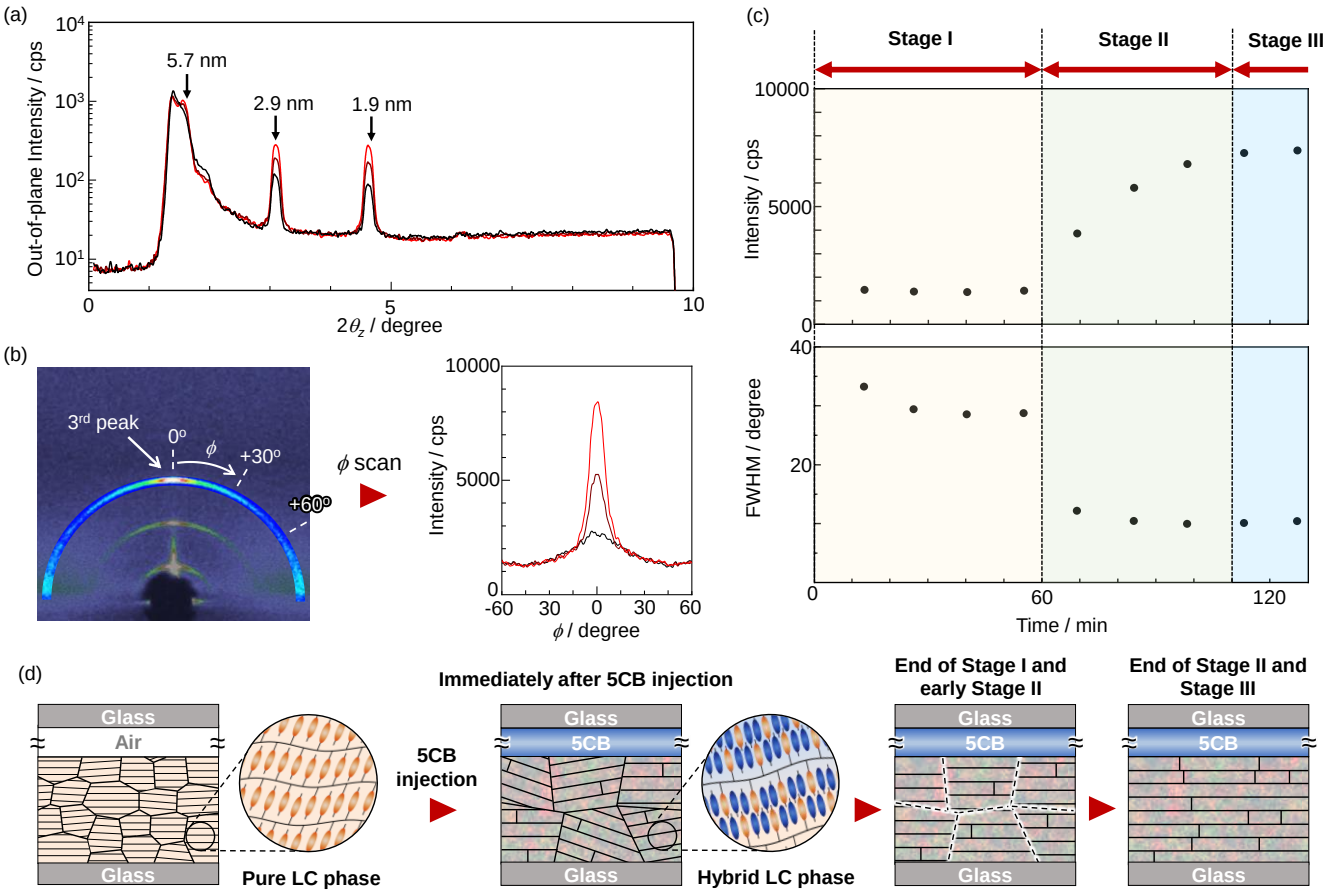

Figure 3. (a) Changes in the out-of-plane intensity profile obtained by SAXS measurements of the 5CB-injected LC cell at 50 °C. Data collected for 14 (black line), 70 (brown), and 128 (red) min after 5CB injection. (b) Left: 2D SAXS image obtained by SAXS measurement of the LC cell at 50 °C in 128 min after 5CB injection. The azimuthal angle (ϕ) scan performed in the 2θ region of the third peak is highlighted. Right: Scattering intensity profiles obtained by the ϕ scan of the third peak in 14 (black line), 70 (brown), and 128 (red) min after 5CB injection. (c) Time course plots of the out-of-plane intensity (upper) and the FWHM value at the azimuthal scan of the third peak (lower). (d) Plausible schematic illustrations of the time-course changes of the hybrid LC phase structure at the three stages after 5CB injection.

Another interesting phenomenon was also observed when the LC cell was cooled down from 50 to 30 °C. The 2D SAXS images and their out-of-plane intensity profiles are shown in Figure 4. In the small-angle region, no significant changes were observed after cooling, however, distinctive scattering peaks with *d*-spacings of 0.45 and 0.40 nm were observed at wide angles in the in-plane direction. These results suggest that a phase transition from the SmA to the SmE phase occurred at temperatures below 40 °C.[56] Similarly, when 5CB was injected into the LC cell at 30 °C, scatterings derived from the SmE phase were directly observed in the wide-angle region (Figure S4). In these ways, the SmE phase is formed independently of the injection temperature. The decreased mobility of 5CB upon cooling caused the phase transition of the hybrid LC phase to the SmE phase.

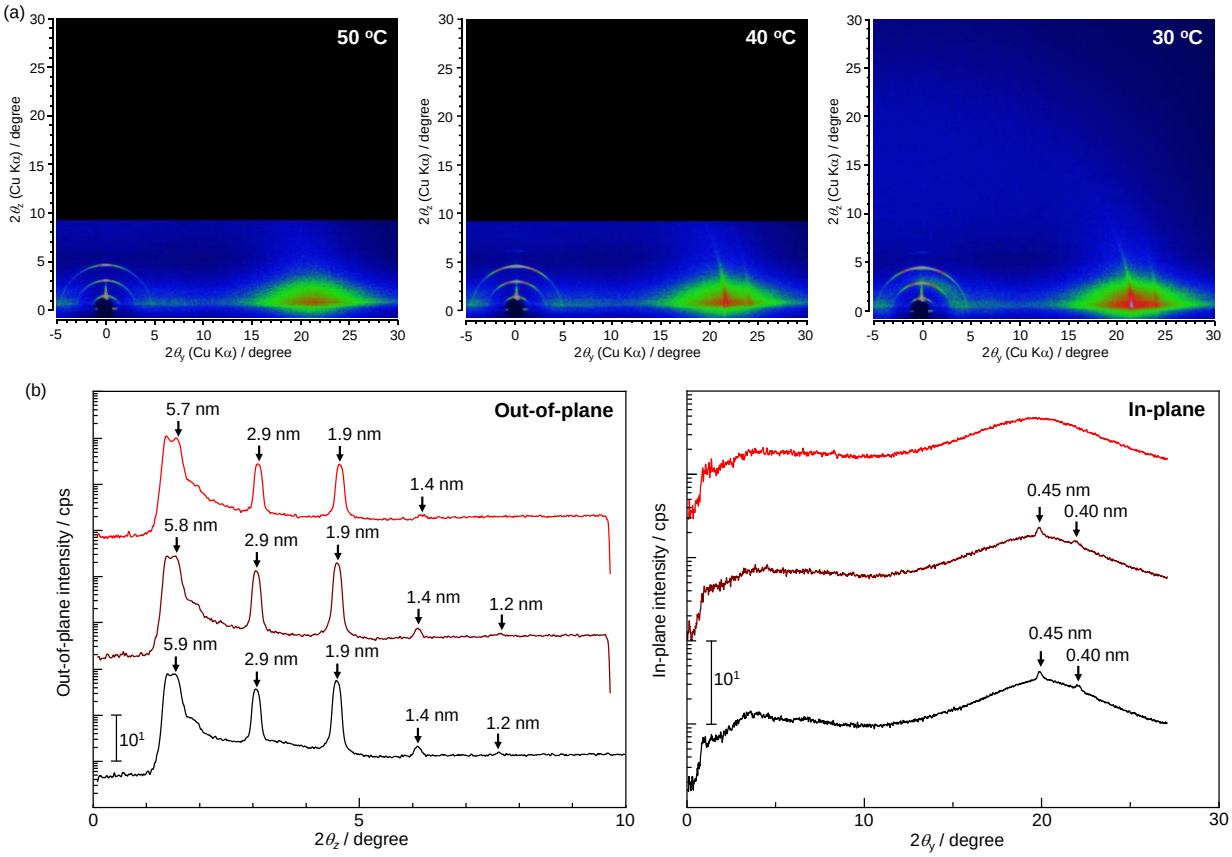

Figure 4. (a) 2D scattering images and (b) intensity profiles obtained by temperature-controlled SAXS measurements of the 5CB-injected LC cell. (red: 50 °C, brown: 40 °C, and black: 30 °C).

Finally, the photoresponsive properties of the hybrid LC phase were examined by UV-light irradiation onto the LC cell at 30 °C. The SAXS data are displayed in Figure 5. As shown, the scattering peaks decreased with increased light dose of UV irradiation, and the peak disappeared after 1.2 J cm^{-2}. In this way, the *trans*-to-*cis* photoisomerization of the Az mesogens led to the phase transition from the SmE to the isotropic phase. Whether 5CB and PAz are phase-separated or mixed as a molecularly compatible state is not elucidated yet. The detailed exploration on the photoresponsive behavior is currently underway.

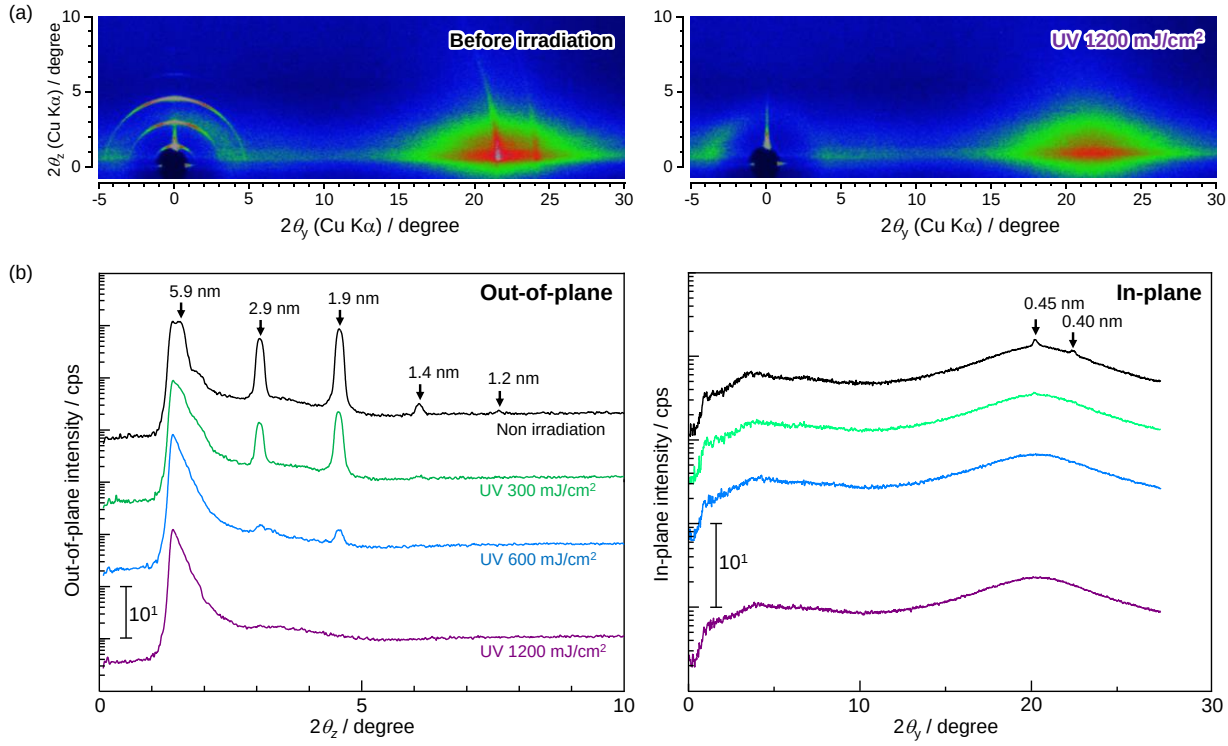

Figure 5. (a) 2D SAXS images of the 5CB-injected LC cell before and after UV irradiation at 30 °C. (b) Out-of-plane and in-plane intensity profiles obtained from the SAXS measurements.

Ubukata et al.[49,50] revealed a strong cooperativity in the light induced orientation changes in hybrid LB films consisting of an amphiphilic Az side chain polymer and 5CB. These data have been obtained in the observations of model systems, and not in an actual photo-command NLC cell. It is to be noted that our present approach enables the in situ time-course X-ray analysis for the intact NLC cell employing our home-made configurated equipment. The key to the successful in situ observations here is that the X-ray signals in the interfacial region are preferentially obtained. In these measurements, the constitution of model film systems is not required. It is anticipated that this experimental strategy can provide real-time structural information also for other types of NLC cells. In the previous work by Ubukata et al.,[49,50] the formation of SmE phase is not elucidated. However, it is probable that even in the previous model LB system such high ordered smectic phase may be formed in consideration of the specific spectral features in the hybrid LB films.

CONCLUSIONS

By evaluating the LC structure inside a 5CB cell coated with the PAz alignment film using specially designed SAXS measurements, we have succeeded in real-time observation of the LC phase near the surface of PAz layer at 50 °C. As a result, a higher-order hybrid SmA phase was induced in the PAz film. This hybrid LC phase was formed immediately after 5CB injection, and was accompanied by an increase in the degree of orientation and domain growth over time. The structural changes can be categorized into three stages. The induced hybrid SmA phase changed into an SmE phase at temperatures below 40 °C. Upon UV light irradiation the SmE phase collapsed to become an isotropic phase. To the best of our knowledge, this is the first report on the spatiotemporal characterization of LC structure close to the vicinity of the alignment layer by X-ray scattering measurements. The photoalignment behavior of NLCs on Az polymer films has still been a subject of extensive studies in recent years.[41-46] Seemingly, the existence of higher-order LC phases in the interface region needs to be considered in each NLC system for precise understandings. The X-ray detection proposed here is expected to effectively contribute to unveil the details of surface alignment behavior for various NLC cells. Probably, this method can be a powerful tool also for the industrial field in terms of failure analysis and new LC device design.

The direct X-ray observations in the intact LC cell system should provide useful information on the driving mechanisms and can expand the utilities for practical applications.

ACKNOWLEDGMENT

We would like to thank Tatsuo Hikage at Nagoya University for his assistance with the X-ray scattering measurements. This work was supported by JSPS KAKENHI, Japan (Grant Numbers JP21H01983 and JP21K19000 to TS and JP22H02142 and JP22H04536 to MH).

Competing interests

The authors declare no competing interests.

Supporting information

The Supporting Information is available free of charge at https://doi.org.

Additional experimental details; Figure S1: SAXS images of the LC cells after injection of 5MB, MBBA and 8CB; Figure S2: Time-course SAXS images of the cells after 5CB injection; Figure S3: Fitting of the azimuth angle intensity profiles; and Figure S4: Out-of-plane and in-plane intensity profiles of the SAXS measurements at 30 °C.

ORCID

Mitsuo Hara: 0000-0003-1829-5153

Shusaku Nagano: 0000-0002-3929-6377

Takahiro Seki: 0000-0003-3010-2641

REFERENCES

1. Wei, W.; Xiong, H. Liquid-Crystalline Polymers: Molecular Engineering, Hierarchical Structures, and Applications. *Langmuir* **2022**, *38*, 11514–11520.

2. Kato, T.; Mizoshita, N.; Kishimoto K. Functional Liquid-Crystalline Assemblies: Self-Organized Soft Materials. *Angew. Chem. Int. Ed.* **2006**, *45*, 38–68.

3. Uchida, J.; Soberats, B.; Gupta, M.; Kato, T. Advanced Functional Liquid Crystals. *Adv. Mater.* **2022**, *34*, 2109063.

4. Tokita, M.; Watanabe, J. Several Interesting Fields Exploited through Understanding of Polymeric Effects on Liquid Crystals of Main-Chain Polyesters. *Polym. J.* **2006**, *38*, 611–638.

5. Lyu, J. J.; Kikuchi, H.; Kim, D. H.; Lee, J. H.; Kim, K. H.; Higuchi, H.; Lee, S. H. Phase separation of monomer in liquid crystal mixtures and surface morphology in polymer-stabilized vertical alignment liquid crystal displays. *J. Phys. D: Appl. Phys.* **2011**, *44*, 325104.

6. Shishido, A. Rewritable holograms based on azobenzene-containing liquid-crystalline polymers. *Polym. J.* **2010**, *42*, 525–533.

7. Iino, H.; Usui, T.; Hanna, J. Liquid crystals for organic thin-film transistors. *Nat. Commun.* **2015**, *6*, 6828.

8. Yu, Y.; Ikeda, T. Soft actuators based on liquid-crystalline elastomers. *Angew. Chem. Int. Ed.* **2006**, *45*, 5416–5418.

9. Creagh, L. T.; Kmetz, A. R. Mechanism of Surface Alignment in Nematic Liquid Crystals. *Mol. Cryst. Liq. Cryst.* **1973**, *24*, 59–68.

10. Seki, T.; Nagano, S.; Hara, M. Versatility of photoalignment techniques: From nematics to a wide range of functional materials. *Polymer* **2013**, *54*, 6053–6072.

11. Wang, M.; Li, Y.; Yokoyama, H. Artificial Web of Disclination Lines in Nematic Liquid Crystals. *Nat. Commun.* **2017**, *8*, 388.

12. Fang, J. Y.; Gehlert, U.; Shashidar, R.; Knobler, C. M. Imaging the Azimuthal Tilt Order in Monolayers by Liquid Crystal Optical Amplification. *Langmuir* **1999**, *15*, 297–299.

13. Drawhorn, R. A.; Abbott, N. L. Anchoring of Nematic Liquid Crystals on Self-Assembled Monolayers Formed from Alkanethiols on Semitransparent Films of Gold. *J. Phys. Chem.* **1995**, *99*, 16511–16515.

14. Noonan, P. S.; Shavit, A.; Acharya, B. R.; Schwartz, D. K. Mixed Alkylsilane Functionalized Surfaces for Simultaneous Wetting and Homeotropic Anchoring of Liquid Crystals. *ACS Appl. Mater. Interfaces* **2011**, *3*, 4374–4380.

15. Bukusoglu, E.; Pantoja, M. B.; Mushenheim, P. C.; Wang, X. G.; Abbott, N. L. Design of Responsive and Active (Soft) Materials Using Liquid Crystals. *Annu. Rev. Chem. Biomol.* **2016**, 7, 163–196.

16. Price, A. D.; Schwartz, D. K. Fatty-Acid Monolayers at the Nematic/Water Interface: Phases and Liquid-Crystal Alignment. *J. Phys. Chem. B* **2007**, *111*, 1007–1015.

17. Khan, M.; Khan, A. R.; Shin, J. H.; Park, S. Y. A liquid-crystal-based DNA biosensor for pathogen detection. *Sci. Rep.* **2016**, *6*, 22676.

18. Xu, Y.; Rather, A. M., Song, S.; Fang, J. C.; Dupont, R. L.; Kara, U. I.; Chang, Y.; Paulson, J. A.; Qin, R.; Bao, X.; Wang, X. Ultrasensitive and Selective Detection of SARS-CoV-2 Using Thermotropic Liquid Crystals and Image-Based Machine Learning. *Cell Rep. Phys. Sci.* **2020**, *1*, 100276.

19. Bates, C. M.; Seshimo, T.; Maher, M. J.; Durand, W. J.; Cushen, J. D.; Dean, L. M.; Blachut, G.; Ellison, C. J.; Willson, C. G. Polarity-switching top coats enable orientation of sub–10-nm block copolymer domains. *Science* **2012**, *338*, 775–779.

20. Ma, J.; Hashimoto, K.; Koganezawa, T.; Tajima, K. End-on orientation of semiconducting polymers in thin films induced by surface segregation of fluoroalkyl chains. *J. Am. Chem. Soc.* **2013**, *135*, 9644–9647.

21. Komura, M.; Yoshitake, A.; Komiyama, H.; Iyoda, T. Control of Air-Interface-Induced Perpendicular Nanocylinder Orientation in Liquid Crystal Block Copolymer Films by a Surface-Covering Method. *Macromolecules* **2015**, 48, 672–678.

22. Gibbons, W. M.; Shannon, P. L.; Sun, S.-T.; Sweltin, B. J. Surface-Mediated Alignment of Nematic Liquid Crystals with Polarized Laser Light. *Nature* **1991**, *351*, 49–50.

23. Kawatsuki, N.; Miyake, K.; Kondo, M. Facile Fabrication, Photoinduced Orientation, and Birefringent Pattern Control of Photoalignable Films Comprised of N-Benzylideneaniline Side Groups. *ACS Macro Lett.* **2015**, *4*, 764–768.

24. Miyake, K.; Ikoma, H.; Okada, M.; Matsui, S.; Kondo, M.; Kawatsuki, N. Orientation Direction Control in Liquid Crystalline Photoalignable Polymeric Films by Adjusting the Free-Surface Condition. *ACS Macro Lett.* **2016**, *5*, 761–765.

25. Xiao, S.; Lu, X.; Lu, Q. Photosensitive Polymer from Ionic Self-Assembly of Azobenzene Dye and Poly(ionic liquid) and Its Alignment Characteristic toward Liquid Crystal Molecules. *Macromolecules* **2007**, *40*, 7944–7950.

26. Chigrinov, V.; Prudnikova, E.; Kozenkov, V.; Kwok, H.; Akiyama, H.; Kawara, T.; Takada, H.; Takatsu, H. Synthesis and properties of azo dye aligning layers for liquid crystal cells. *Liq. Cryst.* **2002**, *29*, 1321–1327.

27. Chigrinov, V.; Kwok, H. S.; Takada, H.; Takatsu, H. Photo-aligning by azo-dyes: physics and applications. *Liq. Cryst. Today*. **2005**, *14*, 1–15.

28. Yaroshchuk, O.; Ho, J.; Chigrinov, V.; Kwok, H.-S. Azodyes as Photoalignment Materials for Polymerizable Liquid Crystals. *Jpn. J. Appl. Phys.* **2007**, *46*, 2995–2998.

29. Kawata, K. Orientation control and fixation of discotic liquid crystal. *Chem. Rec.* **2002**, *2*, 59–80.

30. Goodby, J. W.; Cowling, S. J. Conception, Discovery, Invention, Serendipity and Consortia: Cyanobiphenyls and Beyond. *Crystals* **2022**, *12*, 825.

31. Ichimura, K.; Suzuki, Y.; Seki, T.; Hosoki, A.; Aoki, K. Reversible change in alignment mode of nematic liquid crystals regulated photochemically by command surfaces modified with an azobenzene monolayer. *Langmuir* **1988**, *4*, 1214–1216.

32. Seki, T.; Sakuragi, M.; Kawanishi, Y.; Suzuki, Y.; Tamaki, T.; Fukuda, R.; Ichimura, K. "Command surfaces" of Langmuir-Blodgett films. Photoregulations of liquid crystal alignment by molecularly tailored surface azobenzene layers. *Langmuir* **1993**, *9*, 211-218.

33. Ichimura, K. Photoalignment of Liquid-Crystal Systems. *Chem. Rev*. **2000**, *100*, 1847–1873.

34. Kawanishi, Y.; Suzuki, Y.; Sakuragi, M.; Kamezaki, H.; Ichimura, K. Laser-induced orientational change of nematic liquid crystalline molecules mediated by photochromic reactions of surface azobenzenes. *Photochem. Photobiol. A: Chem.* **1994**, *80*, 433–438.

35. Fukuhara, K.; Nagano, S.; Hara, M.; Seki, T. Liquid-Crystalline Polymer and Block Copolymer Domain Alignment Controlled by Free-Surface Segregation. *Angew. Chem. Int. Ed.* **2013**, *52*, 5988–5991.

36. Fukuhara, K.; Nagano, S.; Hara, M.; Seki, T. Free-surface molecular command systems for photoalignment of liquid crystalline materials. *Nat. Commun.* **2014**, *5*, 3320.

37. Seki, T. A Wide Array of Photoinduced Motions in Molecular and Macromolecular Assemblies at Interfaces. *Bull. Chem. Soc. Jpn.* **2018**, *91*, 1026–1057.

38. Nakai, T.; Tanaka, D.; Hara, M.; Nagano, S.; Seki, T. Free Surface Command Layer for Photoswitchable Out-of-Plane Alignment Control in Liquid Crystalline Polymer Films. *Langmuir* **2016**, *32*, 909–914.

39. Aya, S.; Sasaki, Y.; Takezoe, H.; Ishikawa, K.; Ema, K.; Hikima, T.; Takata, M.; Araoka, F. Stepwise heat-capacity change at an orientation transition in liquid crystals, *Physical Review E* **2014**, 89, 022512.

40. Aya, S.; Sasaki, Y.; Takezoe, H.; Ishikawa, K.; Ema, K.; Hikima, T.; Takata, M.; Araoka, F. Thermodynamically Anchoring-Frustrated Surface to Trigger Bulk Discontinuous Orientational Transition, *Langmuir* **2016**, 32, 10545-10550.

41. Aya, S.; Hikima, T.; Haba, O.; Yonetake, K.; Araoka, F. Dynamics of phototunable two-dimensional polar wetting sheets of a dendritic liquid crystal. *Phys. Rev. E* **2018**, *98*, 052701.

42. Aya, S.; Haba, O.; Yonetake, K.; Araoka, F. Anchoring and molecular conformation of liquid crystalline dendrimer. *J. Mol. Liq.* **2021**, *321*, 114379.

43. Tóth-Katona, T.; Jánossy, I.; Photoalignment at the nematic liquid crystal-polymer interface: Experimental evidence of three-dimensional reorientation. *J. Mol. Liq.* **2019**, *285*, 323–329.

44. Nassrah, A. K. R.; Jánossy, I.; Tóth-Katona, T. Photoalignment at the nematic liquid crystal–polymer interface: The importance of the liquid crystalline molecular structure. *J. Mol. Liq.* **2020**, *312*, 113309.

45. Li, X.; Yanagimachi, T.; Bishop, C.; Smith, C.; Dolejsi, M.; Xie, H.; Kurihara, K.; Nealey, P. F. Engineering the anchoring behavior of nematic liquid crystals on a solid surface by varying the density of liquid crystalline polymer brushes. *Soft Matter* **2018**, *14*, 7569–7577.

46. Kuang, Z.-Y.; Fan, Y.-J.; Tao, L.; Li, M.-L.; Zhao, N.; Wang, P.; Chen, E.-Q.; Fan, F.; Xie, H.-L. Alignment Control of Nematic Liquid Crystal using Gold Nanoparticles Grafted by the Liquid Crystalline Polymer with Azobenzene Mesogens as the Side Chains. *ACS Appl. Mater. Interfaces* **2018**, *10*, 27269–27277.

47. Roscioni, O. M.; Muccioli, L.; Valle, R. G. D.; Pizzirusso, A.; Ricci, M.; Zannoni, C. Predicting the Anchoring of Liquid Crystals at a Solid Surface: 5-Cyanobiphenyl on Cristobalite and Glassy Silica Surfaces of Increasing Roughness. *Langmuir* **2013**, *29*, 8950–8958.

48. Sadati, M.; Ramezani-Dakhel, H.; Bu, W.; Sevgen, E.; Liang, Z.; Erol, C.; Rahimi, M.; Qazvini, N. T.; Lin, B.; Abbott, N. L.; Roux, B.; Schlossman, M. L.; de Pablo, J. J. Molecular Structure of Canonical Liquid Crystal Interfaces. *J. Am. Chem. Soc.* **2017**, *139*, 3841–3850.

49. Ubukata, T.; Seki, T.; Ichimura, K. Modeling the Interface Region of Command Surface 1. Structural Evaluations of Azobenzene/Liquid Crystal Hybrid Langmuir Monolayers. *J. Phys. Chem. B* **2000**, *104*, 4141–4147.

50. Ubukata, T.; Seki, T.; Morino, Sy; Ichimura, K. Modeling the Interface Region of Command Surface 2. Spectroscopic Evaluations of Azobenzene/Liquid Crystal Hybrid Langmuir-Blodgett Films under Illumination. *J. Phys. Chem. B* **2000**, *104*, 4148–4154.

51. Yamakado, R.; Hara, M.; Nagano, S.; Seki, T.; Maeda, H. Photo-Responsive Soft Ionic Crystals: Ion-Pairing Assemblies of Azobenzene Carboxylates. *Chem. Eur. J.* **2017**, *23*, 9244–9248.

52. Furuichi, M.; Hara, M.; Nagano, S.; Seki, T. The Effect of a Topcoat with Amorphous Polymer Layer on the Mesogen Orientation and Photoalignment Behavior of Side Chain Liquie Crystalline Polymer Films, *Appl. Sci.* **2022**, *12*, 9410 (13 pages).

53. Hara, M.; Nagano, S.; Seki, T. Spontaneous Formation of Vertically Aligned Lamellae in Thin Films of Block Copolymer-Silica Hybrid Material. *Bull. Chem. Soc. Jpn.* **2013**, *86*, 1151–1157.

54. Imanishi, R.; Nagashima, Y.; Takishima, K.; Hara, M.; Nagano, S.; Seki, T. Induction of Highly Ordered Smectic Phases in Side Chain Liquid Crystalline Polymers by Means of Random Copolymerization. *Macromolecules* **2020**, *53*, 1942–1949.

55. Sugisawa, S.; Tabe, Y. Induced smectic phases of stoichiometric liquid crystal mixtures. *Soft Matter* **2016**, *12*, 3103–3109.

56. Miyazawa, T.; Yamamura, Y.; Hishida, M.; Nagatomo, S.; Massalska-Arodź, M.; Saito, K. Revisiting Smectic E Structure through Swollen Smectic E Phase in Binary System of 4-Nonyl-4'-isothiocyanatobiphenyl (9TCB) and *n*-Nonane. *J. Phys. Chem. B* **2013**, *117*, 8293–8299.